AIAA JOURNAL
Vol. 44, No. 11, November 2006

Stacking Sequence Design of Flat Composite Panel for Flutter and Thermal Buckling

Omprakash Seresta*
Virginia Polytechnic Institute and State University, Blacksburg, Virigina 24061
Mostafa M. Abdalla†
Delft University of Technology, 2629, HS Delft, The Netherlands
Sameer B. Mulani‡
Virginia Polytechnic Institute and State University, Blacksburg, Virigina 24061
and
Pier Marzocca§
Clarkson University, Potsdam, New York 13699-5725

DOI: 10.2514/1.19532

In this paper, we formulate the stacking sequence design of laminated composite flat panels for maximum supersonic flutter speed and maximum thermal buckling capacity. The design is constrained to have stable limit cycle oscillation in the vicinity of the flutter boundary. For the purpose of comparison, we consider both linear and nonlinear panel flutter analyses. Because of manufacturing constraints, the stacking sequence of the laminate is selected from a discrete set of orientation angles. The plate is modeled using von Kármán plate equations and assumed to be subjected to uniform temperature differential. The aerodynamic load on the plate is computed using third-order piston theory. The plate equations of motion are derived using Hamilton's principle and discretized using the Rayleigh–Ritz method. The nonlinear panel flutter analysis is performed using an approximate perturbation approach. The Pareto fronts describing the trade-off between thermal buckling and flutter are generated for different panel aspect ratios. It is observed that optimal designs obtained for both linear and nonlinear flutter analyses are similar, with only the predicted flutter speeds different. This suggests that, for the purpose of preliminary stacking sequence design, linear flutter analysis is sufficient.

Nomenclature

A_{ij}	=	in-plane stiffness coefficients
a	=	dimension of the panel along x direction, in.
a_∞	=	speed of sound at sea level, in./s
b	=	dimension of the panel along y direction, in.
$\boldsymbol{C}$	=	aerodynamic damping
D_{ij}	=	flexural stiffness coefficients
$\boldsymbol{K}$	=	stiffness matrix
$\boldsymbol{l}, \boldsymbol{r}$	=	left and right eigenvector at the critical Mach number
$\boldsymbol{M}$	=	mass matrix
$M_{L/\mathrm{NL}}$	=	linear or nonlinear flutter Mach number
M_∞	=	flow Mach number
m	=	mass per unit area, lb · s^2·in.$^{-3}$
N_x^T, N_y^T, N_{xy}^T	=	in-plane thermal loads, lb/in.
n	=	number of assumed modes in each direction
Q_A	=	work done by aerodynamic load, lb · in.
Q_{ij}	=	stiffness coefficients
q_∞	=	aerodynamic pressure, psi
T	=	kinetic energy, lb · in.
U	=	strain energy, lb · in.
u	=	displacement along x direction of the panel, in.
U_∞	=	flow velocity, in./s
V_z	=	downwash velocity, in./s
v	=	displacement along y direction of the panel, in.
W	=	total work done, lb · in.
$\bar{W}$	=	work done by thermal load, lb · in.
w	=	displacement along z direction of the panel, in.
Δp	=	pressure distribution, psi
ΔT	=	temperature differential applied to the panel, °F
$\epsilon_x, \epsilon_y, \gamma_{xy}$	=	engineering strain
$\kappa_x, \kappa_y, \kappa_{xy}$	=	bending curvature
$\lambda_{L/\mathrm{NL}}$	=	linear or nonlinear aerodynamic pressure parameter, psi
λ_{cr}^T	=	thermal buckling factor
ρ_∞	=	density of air at sea level, lb · s^2 · in.$^{-4}$
ϕ	=	assumed solution modes

Presented as Paper 2128 at the 46th AIAA/ASME/ASCE/AHS/ASC Structures, Structural Dynamics and Materials Conference, Austin, Texas, 18–21 April 2005; received 17 August 2005; revision received 11 April 2006; accepted for publication 23 June 2006.

*Research Assistant, Department of Aerospace and Ocean Engineering; oseresta@vt.edu. Student Member AIAA.

†Assistant Professor, Aerospace Structures; m.m.abdalla@lr.tudelft.nl. Member AIAA.

‡Research Assistant, Department of Aerospace and Ocean Engineering; smulani@vt.edu. Student Member AIAA.

§Assistant Professor, Department of Mechanical and Aeronautical Engineering; pmarzocc@clarkson.edu. Member AIAA.

I. Introduction

LIFTING surfaces of aerospace vehicles in supersonic or hypersonic regime exhibit two types of flutter. One is classical low-aspect lifting surface flutter and the other is panel flutter. Flutter is defined as the instability associated with increasing amplitudes of oscillation because of the interaction of modes with inertial and aerodynamic coupling. Flutter is a self-sustained oscillation occurring beyond a critical airflow speed in aerospace vehicles. In panel flutter, the dynamic instability occurs when at a specific speed, due to the aerodynamic pressure loads, there is coalescence of two of the structural eigenmodes. At this speed, the damping of the system becomes negative, which leads to ever-increasing oscillation. This aeroelastic instability is of immense concern for aircraft and wing designers as well as for missile designers. Nonlinear effects in aeroelastic systems may be either favorable or unfavorable or a combination of both. For example, when structural stiffness

nonlinearity is equivalent to a hardening spring as in the von Kármán plate model, no limit cycle oscillations (LCO) will exist below the flutter boundary determined in the absence of nonlinearity. And above the flutter speed, the nonlinearity will limit the response, a clearly favorable outcome. However, for other nonlinearities such as structural free play or aerodynamic nonlinearities due to flow separation or large shock motion and very high speed, the effect of nonlinearity may be to induce LCO below the nominal flutter speed, but still limit the LCO response to a finite amplitude both below and above the nominal flutter speed. Whether such nonlinear effects are favorable or not will depend very much on the particular circumstances and parameters involved. Nonetheless, it is clear that nonlinear effects often lead to LCO and in their absence the alternative would be catastrophic failure leading to structural failure.

In the recent years with rapid improvement in manufacturing techniques and need for more specialized materials, the composite materials have gained substantial reputation in the research academia and have widespread applications in aerospace, automotive industries, etc. With their increased use as structural elements due to their high specific strength ratio (strength/weight), much research work is carried on to understand both the linear and nonlinear aeroelastic behavior in this new context. A survey of such studies was given by Dowell [1,2] and Librescu [3]. Librescu studied the aeroelastic response using a standard linearized formulation [4,5]. Chatterjee and Kulkarni [6] studied the effects of shear deformations on flutter of laminated composite plates. Oyibo [7] studied the flutter of orthotropic panels using affine transformations. Birman and Librescu [8] analyzed the supersonic flutter of shear deformable laminated composite plates. In their work, they used the two-dimensional static aerodynamic approximation and a higher-order shear deformation theory for the structural plate model. Dixon and Mei [9] also studied nonlinear flutter of composite panels using finite element methods. Recently, Marzocca et al. [10] used Volterra's approach to predict the aeroelastic response of panels. Aerospace vehicles, such as high-speed aircraft, rockets, and spacecraft, are subjected to thermal loads due to aerodynamic and/or solar radiation heating. This results in a temperature distribution and thermal gradient through the thickness of the plate. Therefore, thermal buckling is a significant failure mode governing the design of thin plates used in aerospace structures. Lee et al. [11] studied the supersonic flutter analysis of stiffened laminated plates subject to thermal load. Liaw studied the linear [12] and nonlinear [13] supersonic flutter of laminated composite plates under thermal loads using finite element method. Cheng and Mei [14] studied panel flutter analysis with thermal effects using finite element modal formulation. For the panel flutter problem in presence of thermal loads, the interested reader is referred to a monograph by Bolotin [15].

Much work has been carried out to optimally design the stacking sequence of laminate configurations to maximize buckling capacity. A comprehensive literature on the optimization of composite laminates for maximization of buckling load can be found in [16–21]. An excellent review on composite laminate optimization is given by Venkataraman and Haftka [22]. However, lesser attempt is made to integrate the advances in aeroelastic concepts within optimization framework. Beiner and Librescu [23] formulated the optimization problem for a shear panel as a minimum weight design with flutter speed constraint. In their work, they formulated weight minimization problems to find the optimum thickness distribution such that the associated flutter speed coincides with that of the reference panel with a uniform thickness. A survey of structural optimization with aeroelastic constraints is given by Haftka [24]. To the authors' knowledge, no attempt is made to simultaneously optimize the stacking sequence of the laminated composite plate for both maximum flutter speed and buckling capacity. The use of laminated composites necessitates the inclusion of fiber orientation angle of the layers as the design variables in the optimization formulation. However, due to manufacturing constraints, the fiber orientation angle of the layers or plies is restricted to 0, ± 45, and 90 deg. Thus, the design variables associated with fiber orientation angle of the plies are discrete in nature.

In this paper, we formulate the laminate stacking sequence optimization of composite plates to maximize the flutter speed and buckling capacity under thermal load. We seek to demonstrate the trade-off between increased flutter velocity and the buckling capacity of the composite laminate. A stability constraint at bifurcation point is introduced to ensure stable equilibrium in the post critical region. To compute the stability behavior in the post critical region, both geometrically nonlinear behavior of the plate and third-order piston theory is considered. The nonlinear panel flutter analysis is computationally expensive. Therefore, a relatively simpler and approximate perturbation approach is employed to compute the nonlinear behavior. For thermal loading, we considered a uniform temperature differential throughout the domain of the plate to keep the computations simple. A genetic algorithm is used as a design optimization platform because of the presence of discrete design variables. The paper is organized as: problem formulation (Sec. II), analysis formulation (Sec. III), optimization formulation (Sec. IV), results (Sec. V), and conclusion.

II. Problem Formulation

A laminated plate of dimension $\underline{a} \times \underline{b}$ in supersonic flow U_∞ (along the x axis only) is considered (Fig. 1). The plate is subjected to uniform temperature variation ΔT. Two modes of failure of the plate can be considered: thermal buckling and supersonic flutter.

The linear flutter Mach number M_L is the value of the freestream M_∞ for which the equilibrium position of the laminate becomes unstable. To be more precise, at the critical Mach number a pair of eigenvalues of the system crosses the imaginary axis. In the mathematics literature, this phenomenon is referred to as Hopf bifurcation. The determination of the critical Mach number depends on the knowledge of the small deflection response of the structure and, as such, is governed by a linear system of equations. If the freestream Mach number M_∞ is increased beyond the critical value, due to the presence of structural nonlinearity stiffness equivalent to a hardening spring of the von Kármán plate model, the panel exhibits self-sustained vibrations referred to as limit cycle oscillations or LCO. In the post-flutter regime, the amplitude of the limit cycle oscillation depends on how far the Mach number is increased beyond the critical value. This type of behavior characterizes stable flutter also known as supercritical Hopf bifurcation. When the flutter is not stable, also known as subcritical Hopf bifurcation, the post-flutter response itself is unstable and the system response can be characterized through time simulations. The amplitude-Mach number relation is controlled by the structural and aerodynamic nonlinearities of the system. Librescu et al. [25] examined the implications of structural and aerodynamic nonlinearities on the determination of stable/unstable LCO and the character of flutter critical boundary. In their work, the behavior in the vicinity of the flutter boundary has been characterized via a Lyapunov-based approach. It was shown that at high flight Mach numbers, cubic aerodynamic nonlinearities contribute invariably toward the catastrophic character of the flutter boundary (unstable LCO)

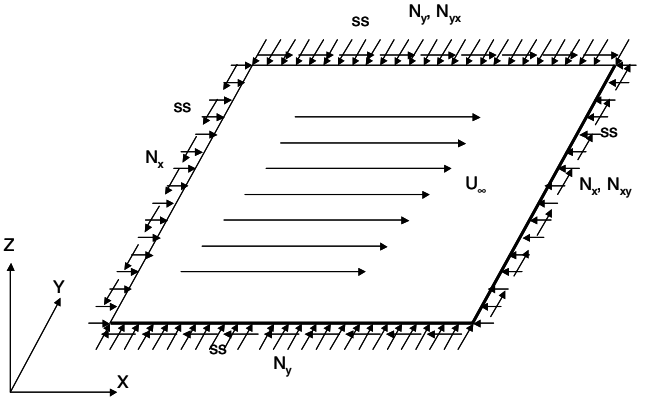

Fig. 1 Plate with coordinate axes, in-plane loads, and boundary conditions.

whereas the quadratic aerodynamic and structural nonlinearities contribute to its benign nature (stable LCO). This implies that with the increase of the supersonic/hypersonic flight speed, the flutter boundary becomes catastrophic, irrespective of the presence of structural and quadratic aerodynamic nonlinearities.

It is thus desirable to design laminates with stable post-flutter response. It is also important that the post-flutter response remains bounded to avoid excessive loading that might lead to failure. For this purpose, a nonlinear flutter speed is usually defined as the Mach number at which the amplitude of the response reaches a predefined value:

$$M_{\mathrm{NL}} = M_L + \delta M \tag{1}$$

where δM is the contribution of structural and aerodynamic nonlinearities.

In the present paper, the value of δM is calculated based on a perturbation method. Because the perturbation method is valid only locally near the Hopf bifurcation, the value of the nonlinear flutter Mach number is only approximate. On the other hand, the use of a perturbation method is advantageous in the sense that a value for δM can be calculated even for unstable flutter. The laminate shows stable bifurcation if δM is positive, whereas a negative value indicates unstable flutter.

For buckling analysis, the laminate is subjected to uniform temperature variation $\lambda^T\,\Delta T$. λ^T_{cr} is the buckling factor for which the laminate buckles. The linear (suffix L) or nonlinear (suffix NL) aerodynamic pressure parameter $\lambda_{L/\mathrm{NL}}$ is defined as

$$\lambda_{L/\mathrm{NL}} = 2q_\infty \Big/ \sqrt{M^2_{L/\mathrm{NL}} - 1}$$

The laminate is optimized to maximize $\lambda_{L/\mathrm{NL}}$ (linear or nonlinear aerodynamic pressure parameter) and λ^T_{cr} (thermal buckling factor). The laminate is made up of N plies with orientations restricted, for manufacturability, to 0, ± 45, and 90 deg. Each ply has a constant thickness t and plies are made up of the same material. Thus, the total thickness of the laminate is $h = Nt$. The laminate is assumed to be symmetric and balanced. Hence, only the half-laminate stacking sequence needs to be considered for the design. The vector of design variables (fiber orientations) is denoted as $\boldsymbol{\Theta}$. Next, the analysis model is developed for moderately large deformation using von Kármán plate theory.

III. Analysis Formulation

A. Modeling

In this subsection, we present a short description of the development of the equations of motion. The flow velocity direction is along the x direction, as shown in Fig. 1. The plate is simply supported and subjected to uniform temperature variation ΔT. Because the laminate is assumed to be symmetric, no thermal moments generate. The equation of motions of the plate is given by Hamilton's principle as [26]

$$\int \delta(T - U + W)\,\mathrm{d}t = 0 \tag{2}$$

Using von Kármán plate theory for moderately large deformation of thin plates, the expressions for T and U can be derived in terms of midplane displacements: $u(x, y, t)$, $v(x, y, t)$, and $w(x, y, t)$. The total external work done comprises work done by aerodynamic load and work done by thermal load. The work done by the aerodynamic load is calculated using third-order piston theory. For more details of calculation, the readers are referred to Appendix B.

Because it is difficult to find an analytical solution, and keeping in view that the primary focus of the work is on design optimization, we adopt a Rayleigh–Ritz method for the purpose of numerical solution. Following the Rayleigh–Ritz procedure, we assume the following displacement fields:

$$w(x, y, t) = \sum_{i=1}^{n} a_i(t)\phi^w_i(x, y), \qquad u(x, y, t) = \sum_{i=1}^{2n} b_i(t)\phi^u_i(x, y)$$
$$v(x, y, t) = \sum_{i=1}^{2n} c_i(t)\phi^v_i(x, y) \tag{3}$$

The functions ϕ^w_i, ϕ^u_i, and ϕ^w_i are chosen such that they satisfy all the specified boundary conditions. The following boundary conditions are assumed:

$$w/u/v(x, 0, t) = w/u/v(x, \underline{b}, t) = w/u/v(0, y, t) = w/u/v(\underline{a}, y, t) = 0 \tag{4}$$

The number of assumed modes for u and v is twice that of lateral displacement in w. This is done to ensure that the in-plane equilibrium is adequately satisfied. Substituting the expression for assumed solutions in the expression of T, U, and W, we get simplified expressions in terms of unknown Ritz coefficients a_i, b_i, and c_i. Using Hamilton's principle and minimizing with respect to Ritz coefficients, the system of equations reduce to the form

$$-g^u_l + K^{ub}_{il} b_i + K^{uc}_{il} c_i + K^{ua}_{ijl} a_i a_j = 0 \quad \forall\ \delta b_l = 0 \tag{5}$$

$$-g^b_l + K^{vb}_{il} b_i + K^{vc}_{il} c_i + K^{va}_{ijl} a_i a_j = 0 \quad \forall\ \delta c_l = 0 \tag{6}$$

$$M_{il}\ddot{a}_i + \bar{K}^s_{il} a_i - \bar{K}^g_{il} a_i + K^{wba}_{ikl} b_i a_k + K^{wca}_{ikl} c_i a_k + \bar{K}^{waa}_{ijkl} a_i a_j a_k + Q_l = 0 \quad \forall\ \delta a_l = 0 \tag{7}$$

where Q_l (the aerodynamic contribution associated with third-order piston theory) is given by

$$Q_l = K^{(1)}_{il} a_i + K^{(2)}_{il} \dot{a}_i + K^{(3)}_{ijl} a_i a_j + K^{(4)}_{ijl} a_i \dot{a}_j + K^{(5)}_{ijl} \dot{a}_i \dot{a}_j + K^{(6)}_{ijkl} a_i a_j a_k + K^{(7)}_{ijkl} a_i a_j \dot{a}_k + K^{(8)}_{ijkl} a_i \dot{a}_j \dot{a}_k + K^{(9)}_{ijkl} \dot{a}_i \dot{a}_j \dot{a}_k \tag{8}$$

The terms mentioned in the preceding equations are given in Appendix C. The first two Eqs. (5) and (6) are linear in the Ritz's coefficient corresponding to in-plane displacements u and v. Thus, the above three Eqs. (5–7) can be reduced into a single equation by eliminating the b_i, and c_i coefficient from Eq. (7) using Eqs. (5) and (6). For details of this condensation process, the reader is referred to Appendix D. The final set of nonlinear panel motion equations governing the plate behavior is given by

$$M_{il}\ddot{a}_i + K_{il} a_i + K_{ijkl} a_i a_j a_k + Q_l = 0 \tag{9}$$

In the current work, we assumed simply supported boundary conditions for the out-of-plane displacements and immovable boundary conditions for the in-plane displacements. These boundary conditions are representative of aerospace panels. The boundary conditions can be easily satisfied by assuming ϕ_i in Eq. (3) for all the displacement components as

$$\phi_i = \sin\frac{\underline{m}\pi x}{\underline{a}} \sin\frac{\underline{n}\pi y}{\underline{b}} \tag{10}$$

where $\underline{m}$ and $\underline{n}$ are integers, $i = \sqrt{n}(\underline{m} - 1) + \underline{n}$, and n is number of terms in the assumed functions. Thus, $\underline{m}$ and $\underline{n}$ varies from $1, 2, \ldots, \sqrt{n}$.

B. Flutter Analysis

The linear panel flutter analysis requires only the linear terms in Eq. (9). Neglecting the higher-order terms, Q_l consists of two parts: aerodynamic stiffness $K^{(1)}$ and aerodynamic damping $K^{(2)}$. Similarly, by neglecting structural nonlinearities, the resultant system of equations reduce to the form

$$[\boldsymbol{M}]\{\ddot{\boldsymbol{a}}\} + [\boldsymbol{K}^{(2)}]\{\dot{\boldsymbol{a}}\} + [\boldsymbol{K} + \boldsymbol{K}^{(1)}]\{\boldsymbol{a}\} = 0 \tag{11}$$

The state space equation is given by

$$\begin{Bmatrix} \dot{\boldsymbol{a}} \\ \ddot{\boldsymbol{a}} \end{Bmatrix} = \begin{bmatrix} [0] & [\boldsymbol{I}] \\ -[\boldsymbol{M}]^{-1}[\boldsymbol{K}+\boldsymbol{K}^{(1)}] & -[\boldsymbol{M}]^{-1}[\boldsymbol{K}^{(2)}] \end{bmatrix} \begin{Bmatrix} \boldsymbol{a} \\ \dot{\boldsymbol{a}} \end{Bmatrix} \tag{12}$$

By varying the flow speed, eigenvalue analysis of the state space equation is performed. The flow speed for which the damping ratio becomes zero is the linear flutter speed.

In aeroelastic problems, unlike structural geometric nonlinearities that are usually stabilizing in nature, the aerodynamic nonlinearities can be destabilizing. Although structural damping can be added, the behavior of the system will not change. To investigate the stability of the post-flutter response, and also to approximate the nonlinear flutter speed, we reduce the equations of motion [Eq. (9)] to the normal form of the Hopf bifurcation [27] in the vicinity of the flutter point. The reduction process can be carried out using either center manifold reduction [27] or, more conveniently, using the method of multiple scales [28]. Following the method of multiple scales (with scales $T_0, T_1, T_2, \ldots$), and using complex variable notation, the state space equation at the flutter point can be written as

$$(\omega^2[\boldsymbol{M}] - i\omega[\boldsymbol{K}^{(2)}] - [\boldsymbol{K}+\boldsymbol{K}^{(1)}])\{\boldsymbol{r}\} = 0 \tag{13}$$

At flutter, that is, $\omega = \omega_f$, the corresponding left and right eigenvectors are given by $\{\boldsymbol{l}\}$ and $\{\boldsymbol{r}\}$, respectively. The eigenvectors are normalized such that

$$\{l\}^T[2i\omega_f(\boldsymbol{M}) + (\boldsymbol{K}^{(2)})]\{\boldsymbol{r}\} = 1 \tag{14}$$

Hence, the complete flutter mode (up to second-order terms) is given by

$$w = \sum_{j=1}^{n} (q r_j \phi_j^w e^{i\omega_f T_0} + \bar{q}\bar{r}_j \phi_j^w e^{-i\omega_f T_0}) \tag{15}$$

where $\bar{r}$ is the complex conjugate of right eigenvector r. The eigenvectors are further normalized such that the maximum deflection is equal to the total laminate thickness. The normal form of the Hopf bifurcation is given as

$$\dot{q} = A_f q \delta U_\infty + B_f q(q\bar{q}) \tag{16}$$

For a maximum amplitude of unity, which means $w_{\max}/h = 1$, the nonlinear contribution to the flutter speed δU_∞ is computed as

$$Re(A_f)\delta U_\infty + Re(B_f) = 0 \tag{17}$$

where

$$A_f = -\{l\}^T \left[\frac{\partial K^{(1)}}{\partial U_\infty}\right]\{r\} \tag{18}$$

and

$$\begin{aligned} B_f = & -K^{\mathrm{NL}}_{ijkl}(r_i\bar{r}_j r_k + \bar{r}_i r_j r_k + r_i r_j \bar{r}_k) l_l \\ & - K^{(4)}_{ijkl}(r_i\bar{r}_j r_k + \bar{r}_i r_j r_k + r_i r_j \bar{r}_k) l_l \\ & - j\omega_f K^{(5)}_{ijkl}(r_i\bar{r}_j r_k + \bar{r}_i r_j r_k - r_i r_j \bar{r}_k) l_l \\ & + \omega_f^2 K^{(6)}_{ijkl}(-r_i\bar{r}_j r_k + \bar{r}_i r_j r_k - r_i r_j \bar{r}_k) l_l \\ & + j\omega_f^3 K^{(7)}_{ijkl}(-r_i\bar{r}_j r_k - \bar{r}_i r_j r_k - r_i r_j \bar{r}_k) l_l \end{aligned} \tag{19}$$

The nonlinear contribution to Mach number at flutter speed, δM, is given as $\delta U_\infty / a_\infty$. The aerodynamic pressure parameter is given as

$$\lambda_{L/\mathrm{NL}} = 2q_\infty \Big/ \sqrt{M^2_{L/\mathrm{NL}} - 1} \tag{20}$$

C. Thermal Buckling Analysis

The standard buckling equation is obtained by neglecting the nonlinear terms, aerodynamic stiffness, and time-dependent terms in Eq. (7) as follows:

$$(\bar{K}^s_{il} - \lambda^T \bar{K}^g_{il}) a_i = 0 \tag{21}$$

The nontrivial solution of Eq. (21) gives the buckling factor λ^T_{cr} computed as the lowest eigenvalue of the preceding system of equation. The corresponding eigenvector gives the buckling mode of the laminated plate.

IV. Optimization Formulation

The multiobjective design optimization problem is usually formulated in two ways. One is the weighted sum of two or more objectives [29]. Another approach is to add the second objective as the constraint and change the constraint margin to generate a Pareto front [29]. In this paper, we followed the second approach. The objective is to maximize the aerodynamic parameter (linear and nonlinear). The second objective, that is, thermal buckling factor, is added as a constraint. Other constraints are ply-contiguity constraint, symmetricity, and balanced condition of the laminate. The design variables are the fiber orientation angles of the layers chosen from a discrete set of 0, ±45, and 90 deg. The optimization problem is stated as

$$\text{maximize } \lambda_{L/\mathrm{NL}}(\boldsymbol{\Theta})$$

subject to

$$\begin{gathered} \delta M \geq 0 \\ \lambda^T_{\mathrm{cr}}(\boldsymbol{\Theta}) \geq \lambda^T_{\mathrm{all}} \\ n_{c0} \leq 4 \\ n_{c90} \leq 4 \\ \text{laminate is symmetric and balanced} \end{gathered}$$

where δM is the contribution due to structural and aerodynamic nonlinearities, $\boldsymbol{\Theta}$ is the stacking sequence of the laminate, and λ^T_{all} is the allowable thermal buckling factor. By varying the value of λ^T_{all}, a Pareto trade-off curve is to be generated.

The symmetric condition of the laminate is taken care of implicitly because only a half-laminate stacking sequence is used as a design variable. The balanced condition of the laminate is taken care of by imposing a penalty on designs violating the constraint. When the number of contiguous plies of the same orientation is large, composite laminates are known to experience matrix cracking. Therefore, a ply-contiguity constraint [16] is imposed so that no more than a certain number of plies of the same fiber orientation angles are allowed successively. In the current formulation, designs with more than four successive 0- (n_{c0}) or 90- (n_{c90}) deg plies are penalized. For ±45-deg plies, the ply contiguity constraint is satisfied automatically.

A standard genetic algorithm (GA) is employed as an optimizer because of the presence of discrete design variables. Genetic algorithm has been applied successfully for stacking sequence design of composite laminate and the field is widely researched [16–21]. Genetic algorithms are probabilistic search algorithms based on natural selection to guide the exploration of design space toward a global optimum. Genetic algorithm, being a probability-based technique, has higher chances to find a global optima when the design space is nonconvex. A typical GA consists of the following steps:

1) Initialize population. GA works with a number of solutions (unlike conventional optimization technique, which works with one solution). The first step is to create a number of solutions (also referred to as a design or individual) randomly, collectively called a population. In the current context, each solution or individual in the population is a laminate lay-up.

2) Rank population. The next step is to rank the individuals according to their performance based on the fitness value (or

Table 1 Comparison of results with Liaw [13].

Stacking sequence	$1/\lambda_{cr}^{T}$	λ_L	λ_L (Liaw [13])	Error (%)	λ_{NL}	λ_{NL} (Liaw [13])	Error (%)
[0/0/0/0]	0.0	342.4	342.0	0.12	387.5	350.0	10.7
[0/0/0/0]	0.5	279.0	280.0	0.36	325.1	300.0	8.4
[90/90/90/90]	0.0	96.2	95.0	1.3	109.6	100.0	9.6
[90/90/90/90]	0.5	59.4	60.0	1.0	75.6	70.0	8.0

Table 2 Optimum laminate configuration for aspect ratio 0.5 and linear flutter analysis

λ_{all}^{T}	Stacking sequence	λ_{cr}^{T}	$\lambda_{\mathbf{L}}$	λ_{NL}
0.0	$[0_2/\pm 45/0/\pm 45_2/90]_s$	3.473	**1621.327**	1888.805
3.4	$[0_2/\pm 45/0/\pm 45_2/90]_s$	3.473	**1621.327**	1888.805
3.6	$[0_2/\pm 45/0/45/90/-45/90_2]_s$	3.647	**1604.430**	1857.178
-	$[0_2/45/0/-45/45/90/-45/90_2]_s$	**3.691**	1213.992	1374.868

Table 3 Optimum laminate configuration for aspect ratio 0.5 and nonlinear flutter analysis

λ_{all}^{T}	Stacking sequence	λ_{cr}^{T}	λ_L	$\lambda_{\mathbf{NL}}$
0.0	$[0_2/45/0/-45/90_2/\pm 45/90]_s$	3.579	1601.026	**1961.074**
3.4	$[0_2/45/0/-45/90_2/\pm 45/90]_s$	3.579	1601.026	**1961.074**
3.6	$[0_2/\pm 45/0/45/90/-45/90_2]_s$	3.647	1604.430	**1857.178**
-	$[0_2/45/0/-45/45/90/-45/90_2]_s$	**3.691**	1213.992	1374.868

Table 4 Optimum laminate configuration for aspect ratio 1 and linear flutter analysis

λ_{all}^{T}	Stacking sequence	λ_{cr}^{T}	$\lambda_{\mathbf{L}}$	λ_{NL}
0.0	$[0_2/\pm 45/45/0/-45/\pm 45/90]_s$	4.316	**1853.969**	2279.193
4.2	$[0_2/\pm 45/45/0/-45/\pm 45/90]_s$	4.316	**1853.969**	2279.193
4.4	$[0_2/\pm 45_3/0/90]_s$	4.448	**1834.094**	2266.484
4.6	$[0/\pm 45/0/\pm 45_2/90_2]_s$	4.655	**1772.250**	2167.307
4.8	$[0/\pm 45_2/0/\pm 45/90_2]_s$	4.807	**1724.517**	2106.043
5.0	$[\pm 45/0/\pm 45/0/45/0/-45/90]_s$	5.010	**1655.882**	2046.280
5.2	$[\pm 45_2/0_2/\pm 45/90_2]_s$	5.222	**1596.280**	1939.052
-	$[\pm 45_5]_s$	**5.582**	1499.747	1772.491

objective function value). This requires evaluation or analysis of each individual.

3) GA operation. A set of GA operators is applied to the population to create a new population. Most common ones are crossover and mutation operator. The first step is to select two individuals from the population, called parents. The most common way of selecting parents for the next generation is roulette-wheel selection based on the probability distribution of the fitness values of the individuals. So the individuals having good fitness value have higher probability of being selected for GA operation. Next, GA operators are applied to produce a child. This process is repeated till the child population has the same size as the parent population.

4) Rank child population. In this step, the fitness of the child population is evaluated and ranked accordingly.

5) Elitist selection. In this step, the new population is formed by selecting individuals from the child and parent populations. The most common way is to select the best solution from the parent population and the rest are from the child population. This ensures that the best design found so far is not lost in the GA operations and continued to be passed from one generation to the next generation.

6) Convergence. The last four steps are repeated till the solution converges or for a certain number of specified iterations. A solution is assumed to have converged if the optimizer fails to find a better solution for a considerable number of iterations.

A Fortran 90 GA framework that was designed in an earlier research effort specifically for composite laminate design is used in the current work [20]. This framework consists of a GA module, encapsulating GA data structures, and a package of GA operators like crossover and mutation. The module, along with the package of operators, constitutes a standard GA. An integer alphabet is used to code ply genes. The implementation details of the GA module and GA packages can be found in the paper by McMahon et al. [20].

Table 5 Optimum laminate configuration for aspect ratio 1 and nonlinear flutter analysis

λ_{all}^{T}	Stacking sequence	λ_{cr}^{T}	λ_L	$\lambda_{\mathbf{NL}}$
0.0	$[0_2/\pm 45/45/0/-45/\pm 45/90]_s$	4.316	1853.969	**2279.193**
4.2	$[0_2/\pm 45/45/0/-45/\pm 45/90]_s$	4.316	1853.969	**2279.193**
4.4	$[0/\pm 45/0_2/\pm 45_2/90]_s$	4.463	1833.482	**2268.518**
4.6	$[0/\pm 45/0/\pm 45/45/0/-45/0]_s$	4.623	1764.415	**2207.086**
4.8	$[\pm 45/0_2/\pm 45/0/\pm 45/90]_s$	4.822	1722.188	**2133.604**
5.0	$[\pm 45/0/\pm 45/0/45/0/-45/90]_s$	5.010	1655.882	**2046.280**
5.2	$[\pm 45_2/0_2/\pm 45/0/90]_s$	5.222	1595.529	**1970.232**
-	$[\pm 45_5]_s$	**5.582**	1499.747	1772.491

V. Results

To evaluate the validity of the solution procedure, a series of linear and nonlinear flutter analyses are performed and compared. In all examples, the number of terms in the assumed displacement is $\underline{m} = \underline{n} = 4$. For these values, the error in the analysis was found to be of acceptable accuracy for preliminary design purposes. To verify the analysis, some of the cases analyzed in Liaw [13] are reproduced.

The example rectangular plate studied is assumed as simply supported with length $\underline{a} = 100$ in. and width $\underline{b} = 50$ in. The laminate configuration is $[\theta/-\theta/-\theta/\theta]$ with thickness of each lamina equal to 0.25 in. The material is boron/epoxy with the following properties: $E_1 = 10.0$ Mpsi, $E_2 = 1.0$ Mpsi, $G_{12} = 0.33$ Mpsi, $\nu_{12} = 0.3$, $\rho = 0.145 \times 10^{-3}$ lb $\cdot$ s$^2\cdot$in.$^{-4}$, $\alpha_1 = 1.0 \times 10^{-6}$ in. in.$^{-1}/^\circ$F, and $\alpha_2 = 2.0 \times 10^{-6}$ in. in.$^{-1}/^\circ$F. The following value of air density and speed of sound at sea level is used: $\rho_\infty = 1.208 \times 10^{-6}$ lb $\cdot$ s$^2\cdot$in.$^{-4}$, and $a_\infty = 12990$ in./s. In Table 1, a comparison of results with Liaw [13] is presented for $w_{\max}/h = 0.25$. It is seen that the difference between the results for linear analysis is well below 2%. In accordance with Liaw [13], only structural nonlinearity is considered for the purpose of comparison of nonlinear panel flutter analysis. The discrepancy in nonlinear analysis is about 10%. For cases $1/\lambda^T_{\rm cr} \le 0.5$ and $w_{\max}/h \le 0.25$, the quality of our approximate analysis is deemed representative enough of the panel behavior and can be used for optimization.

A. Stacking Sequence Optimization

The stacking sequence design optimization problem is investigated for four cases of laminated plates with aspect ratios 0.5, 1, 2, and 3. All plates have a side length of 50 in. normal to the flow direction except the first one, where the side length is 100 in. All plates are subject to a uniform temperature differential equal to 100°F. The GA parameters used for the optimization run are: number of individuals in a population, 20; probability of crossover, 1.0; probability of mutation, 0.05; and number of elites retained in the population, 1; and number of iterations, 50. The total number of plies in each laminate is equal to 20 and ply thickness is 0.05 in. In all the tabulated results, the corresponding objective function is in bold.

The optimum laminate configurations for plates with aspect ratio of 0.5 for linear and nonlinear panel flutter are given in Table 2 and 3. The first row lists the design optimized for maximum flutter speed, and the last row lists the design optimized for maximum thermal buckling load. The intermediate results are obtained by optimizing the panel for maximum flutter speed and a minimum thermal buckling constraint, as discussed in Sec. IV.

The flutter optimized deign, using linear flutter analysis, has a linear flutter parameter λ_L of 1621.327 and a critical thermal buckling ratio $\lambda^T_{\rm cr}$ of 3.473. The buckling optimized design has a linear flutter parameter λ_L of 1213.992 and a thermal buckling parameter $\lambda^T_{\rm cr}$ of 3.691. Thus, over the Pareto front, the linear flutter pressure varies approximately within 25% of its maximum value, the nonlinear flutter speed varies within approximately 27%, and the thermal buckling load varies within approximately 6% of its maximum value. For the flutter optimized designs using nonlinear flutter analysis (Table 3), the range of nonlinear flutter parameter is 30%, linear flutter parameter is 24%, and thermal buckling is 3%. These results indicate a much stronger sensitivity of flutter performance compared with thermal buckling. The maximum difference in the nonlinear flutter parameter between designs optimized for linear and nonlinear analysis is approximately 4%. The corresponding maximum difference in the linear flutter parameter is approximately 1%. The optimal stacking sequences for linear and nonlinear flutter analyses are similar but not identical.

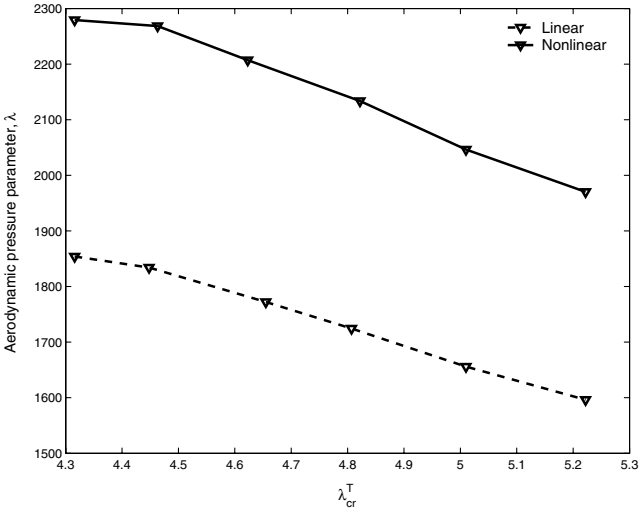

Fig. 2 Trade-off between aerodynamic pressure parameter and buckling capacity for aspect ratio 1.

The optimum laminate configuration for a panel of aspect ratio 1 for linear and nonlinear panel flutter analyses are given in Tables 4 and 5. Unlike the previous case, here thermal buckling and flutter performance show a much stronger competition. The range of thermal buckling parameter and flutter speed are both approximately 20% of their respective maxima. The strong trade-off in design can be attributed to the difference in tailoring requirements of the bending stiffness for flutter and thermal buckling. For example, the difference in designs when $\lambda^T_{\rm all}$ is increased from 4.2 to 4.4 in Table 4. Here, in both cases, the number of 0, ± 45, and 90 plies is the same, implying the in-plane stiffness coefficients are identical. The difference in stacking sequence implies a change in bending stiffness coefficients. The difference in bending stiffness is reflected in the increase of buckling capacity by 3.6%, and decrease in λ_L by 1.1%. The trade-off between critical aerodynamic pressure and buckling capacity is almost linear, as shown in Fig. 2. The optimal designs or laminate lay-ups obtained for linear and nonlinear panel flutter analyses is different in some cases. But this difference, as mentioned in the previous case, is not significant in the sense that the flutter parameter values are close, the difference being less than 2%.

For plates with aspect ratio 2, the optimum laminate configuration is given in Table 6. Also in this case, we observed that the optimum designs obtained using linear and nonlinear flutter analyses are exactly identical. This does not necessarily imply that the objective function contours for linear and nonlinear are identical and could be the result of the discrete nature of the design problem. The trade-off between critical aerodynamic pressure parameter and buckling capacity is no longer linear, as shown in Fig. 3. Initially, the Pareto curve is very flat, suggesting insensitiveness to increased buckling constraint, but after a certain point the aerodynamic pressure parameter decreases rapidly. The range of flutter and thermal

Table 6 Optimum laminate configuration for aspect ratio 2 and both linear and nonlinear flutter analyses

$\lambda^T_{\rm all}$	Stacking sequence	$\lambda^T_{\rm cr}$	$\lambda_{\rm L}$	$\lambda_{\rm NL}$
0.0	$[\pm 45_4/90_2]$	2.769	**511.463**	545.969
2.6	$[\pm 45_4/90_2]$	2.769	**511.463**	545.969
2.8	$[\pm 45_5]_s$	2.959	**507.313**	542.569
3.2	$[\pm 45_4/0_2]_s$	3.203	**497.839**	538.777
3.3	$[\pm 45/90/\pm 45/45/0/-45/0_2]_s$	3.361	**408.249**	449.158
3.4	$[45/90/-45/\pm 45/45/0/-45/0_2]_s$	3.421	**384.222**	424.820
3.5	$[90/\pm 45_2/45/0/-45/0_2]_s$	3.508	**359.302**	399.224
-	$[90_2/45/90/-45/45/0/-45/0_2]_s$	**3.691**	201.180	237.240

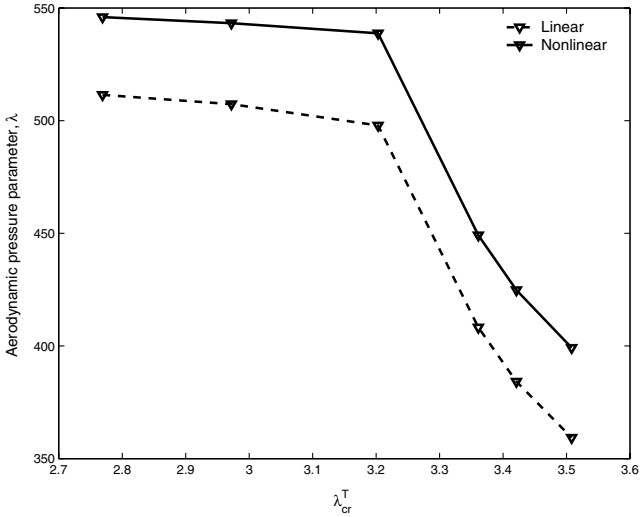

Fig. 3 Trade-off between aerodynamic pressure parameter and buckling capacity for aspect ratio 2.

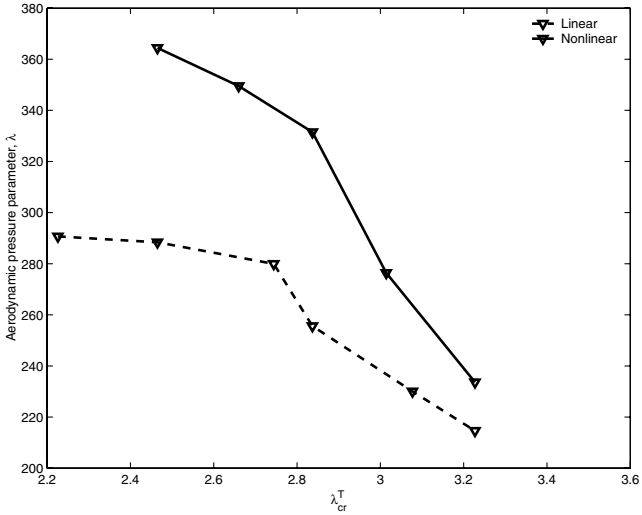

Fig. 4 Trade-off between aerodynamic pressure parameter and buckling capacity for aspect ratio 3.

buckling parameters is approximately 60 and 25% of their respective maximum values.

The optimal laminate configuration for plates with aspect ratio 3 is given in Tables 7 and 8. The optimal designs for linear panel flutter and nonlinear panel flutter are different, particularly for case $\lambda_{\text{all}}^{T} = 2.6$ and 3.0. For all the other cases, the difference is either very small or not present at all. From Fig. 4, we see that the trade-off follows the same pattern found in the case of aspect ratio 2. The range of thermal buckling and flutter parameters with respect to their maximum values is also similar.

VI. Conclusion

In this paper, we formulated the laminate configuration optimization of flat composite panels for both maximum flutter speed (flutter aerodynamic pressure parameter) and maximum thermal buckling capacity with stability constraint on the post-flutter response. The panel equations of motion are developed using third-order piston theory including structural geometric nonlinearities. A semianalytical method of solution is adopted, and a perturbation approach is used to compute the flutter stability constraint and approximate the nonlinear flutter speed. The trade-off between thermal buckling load and aerodynamic pressure parameter is investigated, and the effect of aspect ratio of the plate is also studied. It is observed that there exists an almost linear trade-off between aerodynamic pressure parameter and thermal buckling capacity of square panels. For rectangular plates, this is no longer true, and the trade-off is nonlinear. Also, we compared the optimum designs obtained using linear and nonlinear flutter analyses. For the example problems considered, the optimal stacking sequences are found to be weakly dependent on the consideration of nonlinearity in predicting the flutter speed. It is concluded that although linear flutter analysis significantly underestimates flutter speed as compared with nonlinear calculations, for panel optimization purposes, linear flutter analysis should be sufficient.

Appendix A: Composite Laminate Analysis

The reduced stiffness coefficients of the orthotropic layers are given in terms of engineering constant of the materials as

$$Q_{11} = \frac{E_1}{1-\nu_{12}\nu_{21}}, \qquad Q_{12} = \frac{\nu_{21}E_1}{1-\nu_{12}\nu_{21}} = \frac{\nu_{12}E_2}{1-\nu_{12}\nu_{21}}$$

$$Q_{22} = \frac{E_2}{1-\nu_{12}\nu_{21}}, \qquad Q_{66} = G_{12}$$

Table 7 Optimum laminate configuration for aspect ratio 3 and linear flutter analysis

λ_{all}^{T}	Stacking sequence	λ_{cr}^{T}	λ_{L}	λ_{NL}
0.0	$[\pm 45_3/0/\pm 45/90]_s$	2.226	**290.663**	360.671
2.2	$[\pm 45_3/0/\pm 45/90]_s$	2.226	**290.663**	360.671
2.4	$[\pm 45_3/0/45/0/-45]_s$	2.465	**288.399**	364.445
2.6	$[\pm 45_3/0_4]_s$	2.744	**279.962**	299.416
2.8	$[\pm 45/45/90/-45/\pm 45/0_3]_s$	2.837	**255.632**	331.516
3.0	$[45/90/-45/\pm 45_2/0_3]_s$	3.077	**230.037**	249.210
3.2	$[90/\pm 45_3/0_3]_s$	3.227	**214.629**	233.645
-	$[90_2/45/90/-45/45/0/-45/0_2]_s$	**3.690**	118.007	136.252

Table 8 Optimum laminate configuration for aspect ratio 3 and nonlinear flutter analysis.

λ_{all}^{T}	Stacking sequence	λ_{cr}^{T}	λ_{L}	λ_{NL}
0.0	$[0_2/\pm 45/45/0/-45/\pm 45/90]_s$	2.465	288.399	**364.445**
2.4	$[0_2/\pm 45_3/0/90]_s$	2.465	288.399	**364.445**
2.6	$[\pm 45_2/45/90/-45/0_3]_s$	2.660	271.987	**349.509**
2.8	$[\pm 45/45/90/-45/\pm 45/0_3]_s$	2.837	255.632	**331.516**
3.0	$[90/\pm 45_2/45/90/-45/0_2]_s$	3.014	211.841	**276.399**
3.2	$[90/\pm 45_3/0_3]_s$	3.227	214.629	**233.645**
-	$[90_2/45/90/-45/45/0/-45/0_2]_s$	**3.690**	118.007	136.252

The transformed reduced stiffness of an orthotropic layer with fiber orientation at an angle of θ is given as

$$\begin{aligned}
\bar{Q}_{11}&=Q_{11}\cos^4\theta + 2(Q_{12}+2Q_{66})\sin^2\theta\cos^2\theta + Q_{22}\sin^4\theta,\\
\bar{Q}_{12}&= (Q_{12}+Q_{22}-4Q_{66})\sin^2\theta\cos^2\theta + Q_{12}(\cos^4\theta+\sin^4\theta),\\
\bar{Q}_{22}&= Q_{11}\sin^4\theta + 2(Q_{12}+2Q_{66})\sin^2\theta\cos^2\theta + Q_{22}\cos^4\theta,\\
\bar{Q}_{16}&= (Q_{11}-Q_{22}-2Q_{66})\sin\theta\cos^3\theta\\
&\quad + (Q_{12}-Q_{22}+2Q_{66})\sin^3\theta\cos\theta,\\
\bar{Q}_{26}&= (Q_{11}-Q_{22}-2Q_{66})\sin^3\theta\cos\theta\\
&\quad + (Q_{12}-Q_{22}+2Q_{66})\sin\theta\cos^3\theta,\\
Q_{66}&= (Q_{11}+Q_{22}-2Q_{12}-2Q_{66})\cos^2\theta\sin^2\theta\\
&\quad + Q_{66}(\cos^4\theta+\sin^4\theta)
\end{aligned}$$

The in-plane and flexural stiffnesses are given as

$$A_{ij}=\sum_{k=1}^{N}(\bar{Q}_{ij})_k(z_k-z_{k-1}),\qquad D_{ij}=\sum_{k=1}^{N}(\bar{Q}_{ij})_k(z_k^3-z_{k-1}^3)$$

Appendix B: Plate Model for Moderately Large Deformation

The thermal forces generated due to uniform temperature differential ΔT are given by

$$\begin{Bmatrix} N_x^T\\ N_y^T\\ N_{xy}^T\end{Bmatrix}=\sum_{k=1}^{N}\int_{z_{k-1}}^{z_k}\begin{bmatrix}\bar{Q}_{11}&\bar{Q}_{12}&\bar{Q}_{16}\\ \bar{Q}_{12}&\bar{Q}_{22}&\bar{Q}_{26}\\ \bar{Q}_{16}&\bar{Q}_{26}&\bar{Q}_{66}\end{bmatrix}_k\begin{Bmatrix}\bar{\alpha}_1\\ \bar{\alpha}_2\\ \bar{\alpha}_6\end{Bmatrix}_k\Delta T\,\mathrm{d}z$$

where $(\bar{Q}_{ij})_k$ are the reduced stiffness coefficients given in terms of engineering constants of the material and the fiber orientation angle of the kth layer (see Appendix A), and $(\bar{\alpha}_i)_k$ are the transformed material coefficients.

Assuming that the plate is thin, such that the Kirchoff hypothesis is valid, the in-plane strain components are given by

$$\epsilon_x=\epsilon_x^0+z\kappa_x,\qquad \epsilon_y=\epsilon_y^0+z\kappa_y,\qquad \gamma_{xy}=\gamma_{xy}^0+z\kappa_{xy}$$

The superscript 0 indicates the associated quantity at the midsurface. Using von Kármán equations, the midplane strain vector in terms of midplane displacements u, v, and w is given by

$$\begin{Bmatrix}\epsilon_x^0\\ \epsilon_y^0\\ \gamma_{xy}^0\end{Bmatrix}=\begin{Bmatrix}u_{,x}+\frac{1}{2}w_{,x}^2\\ v_{,y}+\frac{1}{2}w_{,y}^2\\ u_{,y}+v_{,x}+w_{,x}w_{,y}\end{Bmatrix}$$

The bending curvature vector is given by

$$\begin{Bmatrix}\kappa_x\\ \kappa_y\\ \kappa_{xy}\end{Bmatrix}=\begin{Bmatrix}-w_{,xx}\\ -w_{,yy}\\ -2w_{,xy}\end{Bmatrix}$$

The subscripts x and y denote space derivative with respect to the variables x and y.

The kinetic energy is given by

$$T=\frac{1}{2}\int_0^a\int_0^b m\left(\frac{\partial w}{\partial t}\right)^2\mathrm{d}x\,\mathrm{d}y$$

The strain energy of symmetric and balanced laminate is given by

$$\begin{aligned}
U=\frac{1}{2}\int_0^a\int_0^b&[A_{11}(\epsilon_x^0)^2+2A_{12}\epsilon_x^0\epsilon_y^0+A_{22}(\epsilon_y^0)^2+A_{66}(\gamma_{xy}^0)^2\\
&+D_{11}\kappa_x^2+2D_{12}\kappa_x\kappa_y+D_{22}\kappa_y^2+2D_{16}\kappa_x\kappa_{xy}+2D_{26}\kappa_y\kappa_{xy}\\
&+D_{66}\kappa_{xy}^2]\,\mathrm{d}x\,\mathrm{d}y
\end{aligned}$$

where the in-plane stiffnesses A_{11}, A_{12}, A_{22}, and A_{66}, and the flexural stiffnesses $D_{11}, D_{12}, D_{22}, D_{16}, D_{26}$ and D_{66} of the laminate, are given in terms of engineering constants of the material (see Appendix A). The work done by the aerodynamic load is given in terms of pressure distribution by

$$Q_A=\int_0^a\int_0^b\Delta p\,w(x,y,t)\,\mathrm{d}x\,\mathrm{d}y$$

and the work done by the thermal load is given by

$$\bar{W}=\int_0^a\int_0^b(N_x^T\epsilon_x^0+N_y^T\epsilon_y^0+N_{xy}^T\gamma_{xy}^0)\,\mathrm{d}x\,\mathrm{d}y$$

Thus, the total work done by external load is given by

$$W=Q_A+\bar{W}$$

The pressure distribution on an initially flat panel using third-order piston theory is given in terms of density of air, speed of sound, and downwash velocity as [25,30],

$$\Delta p=\rho_\infty a_\infty^2\left(\frac{V_z}{a_\infty}+\frac{1}{2}\frac{V_z^2}{a_\infty^2}+\frac{1}{6}\frac{V_z^3}{a_\infty^3}\right)$$

The downwash velocity is given in terms of flow velocity and lateral displacement as

$$V_z=U_\infty\frac{\partial w}{\partial x}+\frac{\partial w}{\partial t}$$

Appendix C: Full Form of the Tensors that Appear in the Model

The terms in Eqs. (5–7), are given as

$$g_l^u=\int_0^a\int_0^b[N_x^T\phi_{l,x}^u+N_{xy}^T\phi_{l,y}^u]\,\mathrm{d}x\,\mathrm{d}y$$

$$g_l^v=\int_0^a\int_0^b[N_y^T\phi_{l,y}^v+N_{xy}^T\phi_{l,x}^v]\,\mathrm{d}x\,\mathrm{d}y$$

$$K_{il}^{ub}=\int_0^a\int_0^b[A_{11}\phi_{i,x}^u\phi_{l,x}^u+A_{66}\phi_{i,y}^u\phi_{l,y}^u]\,\mathrm{d}x\,\mathrm{d}y$$

$$K_{il}^{uc}=\int_0^a\int_0^b[A_{12}\phi_{i,y}^v\phi_{l,x}^u+A_{66}\phi_{i,x}^v\phi_{l,y}^u]\,\mathrm{d}x\,\mathrm{d}y$$

$$\begin{aligned}
K_{ijl}^{ua}=\tfrac{1}{2}\int_0^a\int_0^b&[A_{11}\phi_{i,x}^w\phi_{j,x}^w\phi_{l,x}^u+A_{12}\phi_{i,y}^w\phi_{j,y}^w\phi_{i,x}^u+A_{66}\phi_{i,x}^w\phi_{j,y}^w\phi_{l,y}^u\\
&+A_{66}\phi_{i,y}^w\phi_{j,x}^w\phi_{l,y}^u]\,\mathrm{d}x\,\mathrm{d}y
\end{aligned}$$

$$K_{il}^{vb}=\int_0^a\int_0^b[A_{12}\phi_{i,x}^u\phi_{l,y}^v+A_{66}\phi_{i,y}^u\phi_{l,x}^v]\,\mathrm{d}x\,\mathrm{d}y$$

$$K_{il}^{vc}=\int_0^a\int_0^b[A_{22}\phi_{i,y}^v\phi_{l,y}^v+A_{66}\phi_{i,x}^v\phi_{l,x}^v]\,\mathrm{d}x\,\mathrm{d}y$$

$$\begin{aligned}
K_{ijl}^{va}=\tfrac{1}{2}\int_0^a\int_0^b&[A_{12}\phi_{i,x}^w\phi_{j,x}^w\phi_{l,y}^v+A_{22}\phi_{i,y}^w\phi_{j,y}^w\phi_{l,y}^v+A_{66}\phi_{i,x}^w\phi_{j,y}^w\phi_{l,x}^v\\
&+A_{66}\phi_{i,y}^w\phi_{j,x}^w\phi_{l,x}^v]\,\mathrm{d}x\,\mathrm{d}y
\end{aligned}$$

$$M_{il} = \int_0^{\underline{a}} \int_0^{\underline{b}} m\phi_i^w \phi_l^w \, \mathrm{d}x \, \mathrm{d}y$$

$$\begin{aligned}\bar{K}_{il} = \int_0^{\underline{a}} \int_0^{\underline{b}} [&D_{11}\phi_{i,xx}^w \phi_{l,xx}^w + D_{12}\phi_{i,yy}^w \phi_{l,xx}^w + D_{12}\phi_{i,xx}^w \phi_{l,yy}^w \\ &+ D_{22}\phi_{i,yy}^w \phi_{l,yy}^w + 2D_{16}\phi_{i,xy}^w \phi_{l,xx}^w + 2D_{16}\phi_{i,xx}^w \phi_{l,xy}^w \\ &+ 2D_{26}\phi_{i,xy}^w \phi_{l,yy}^w + 2D_{26}\phi_{i,yy}^w \phi_{l,xy}^w + 4D_{66}\phi_{i,xy}^w \phi_{l,xy}^w] \, \mathrm{d}x \, \mathrm{d}y\end{aligned}$$

$$\begin{aligned}\bar{K}_{il}^g = \int_0^{\underline{a}} \int_0^{\underline{b}} [&N_x^T \phi_{i,x}^w \phi_{l,x}^w + N_y^T \phi_{i,y}^w \phi_{l,x}^w \\ &+ N_{xy}^T (\phi_{i,y}^w \phi_{l,x}^w + \phi_{i,x}^w \phi_{l,y}^w)] \, \mathrm{d}x \, \mathrm{d}y\end{aligned}$$

$$\begin{aligned}K_{ikl}^{wba} = \int_0^{\underline{a}} \int_0^{\underline{b}} [&A_{11}\phi_{i,x}^u \phi_{k,x}^w \phi_{l,x}^w + A_{12}\phi_{i,x}^u \phi_{k,y}^w \phi_{l,y}^w + A_{66}\phi_{i,y}^u \phi_{k,y}^w \phi_{l,x}^w \\ &+ A_{66}\phi_{i,y}^u \phi_{k,x}^w \phi_{l,y}^w] \, \mathrm{d}x \, \mathrm{d}y\end{aligned}$$

$$\begin{aligned}K_{ikl}^{wca} = \int_0^{\underline{a}} \int_0^{\underline{b}} [&A_{12}\phi_{i,y}^v \phi_{k,x}^w \phi_{l,x}^w + A_{22}\phi_{i,y}^v \phi_{k,y}^w \phi_{l,y}^w + A_{66}\phi_{i,x}^v \phi_{k,y}^w \phi_{l,x}^w \\ &+ A_{66}\phi_{i,x}^v \phi_{k,x}^w \phi_{l,y}^w] \, \mathrm{d}x \, \mathrm{d}y\end{aligned}$$

$$\begin{aligned}\bar{K}_{ijkl}^{waa} = \frac{1}{2} \int_0^{\underline{a}} \int_0^{\underline{b}} [&A_{11}\phi_{i,x}^w \phi_{j,x}^w \phi_{k,x}^w \phi_{l,x}^w + A_{12}\phi_{i,y}^w \phi_{j,y}^w \phi_{k,x}^w \phi_{l,x}^w \\ &+ A_{12}\phi_{i,x}^w \phi_{j,x}^w \phi_{k,y}^w \phi_{l,y}^w + A_{22}\phi_{i,y}^w \phi_{j,y}^w \phi_{k,y}^w \phi_{l,y}^w \\ &+ A_{66}\phi_{i,x}^w \phi_{j,y}^w \phi_{k,y}^w \phi_{l,x}^w + A_{66}\phi_{i,x}^w \phi_{j,y}^w \phi_{k,x}^w \phi_{l,y}^w \\ &+ A_{66}\phi_{i,y}^w \phi_{j,x}^w \phi_{k,y}^w \phi_{l,x}^w + A_{66}\phi_{i,y}^w \phi_{j,x}^w \phi_{k,x}^w \phi_{l,y}^w] \, \mathrm{d}x \, \mathrm{d}y\end{aligned}$$

$$K_{il}^{(1)} = \rho_\infty a_\infty^2 M_\infty \int_0^{\underline{a}} \int_0^{\underline{b}} \phi_{i,x}^w \phi_l^w \, \mathrm{d}x \, \mathrm{d}y$$

$$K_{il}^{(2)} = \rho_\infty a_\infty \int_0^{\underline{a}} \int_0^{\underline{b}} \phi_i^w \phi_l^w \, \mathrm{d}x \, \mathrm{d}y$$

$$K_{ijl}^{(3)} = \tfrac{1}{2}\rho_\infty a_\infty^2 M_\infty^2 \int_0^{\underline{a}} \int_0^{\underline{b}} \phi_{i,x}^w \phi_{j,x}^w \phi_l^w \, \mathrm{d}x \, \mathrm{d}y$$

$$K_{ijl}^{(4)} = \rho_\infty a_\infty M_\infty \int_0^{\underline{a}} \int_0^{\underline{b}} \phi_{i,x}^w \phi_j^w \phi_l^w \, \mathrm{d}x \, \mathrm{d}y$$

$$K_{ijl}^{(5)} = \tfrac{1}{2}\rho_\infty \int_0^{\underline{a}} \int_0^{\underline{b}} \phi_i^w \phi_j^w \phi_l^w \, \mathrm{d}x \, \mathrm{d}y$$

$$K_{ijkl}^{(6)} = \frac{\rho_\infty a_\infty^2 M_\infty^3}{6} \int_0^{\underline{a}} \int_0^{\underline{b}} \phi_{i,x}^w \phi_{j,x}^w \phi_{k,x}^w \phi_l^w \, \mathrm{d}x \, \mathrm{d}y$$

$$K_{ijkl}^{(7)} = \frac{\rho_\infty a_\infty M_\infty^2}{2} \int_0^{\underline{a}} \int_0^{\underline{b}} \phi_{i,x}^w \phi_{j,x}^w \phi_k^w \phi_l^w \, \mathrm{d}x \, \mathrm{d}y$$

$$K_{ijkl}^{(8)} = \frac{\rho_\infty M_\infty}{2} \int_0^{\underline{a}} \int_0^{\underline{b}} \phi_{i,x}^w \phi_j^w \phi_k^w \phi_l^w \, \mathrm{d}x \, \mathrm{d}y$$

$$K_{ijkl}^{(9)} = \frac{\rho_\infty}{6a_\infty} \int_0^{\underline{a}} \int_0^{\underline{b}} \phi_i^w \phi_j^w \phi_k^w \phi_l^w \, \mathrm{d}x \, \mathrm{d}y$$

Appendix D: Condensation Procedure

The Eqs. (6) and (7) are condensed by assuming the following:

$$\{\boldsymbol{e}\} = \begin{Bmatrix} \{\boldsymbol{b}\} \\ \{\boldsymbol{c}\} \end{Bmatrix}$$

$$\{\boldsymbol{g}\} = \begin{Bmatrix} \{\boldsymbol{g}\}u \\ \{\boldsymbol{g}\}v \end{Bmatrix}$$

$$[\boldsymbol{K}] = \begin{bmatrix} [\boldsymbol{K}^{ub}] & [\boldsymbol{K}^{uc}] \\ [\boldsymbol{K}^{vb}] & [\boldsymbol{K}^{vc}] \end{bmatrix}$$

$$K_{ijp}^{ab} = \begin{cases} K_{ijl}^{uaa} & \text{for } p = 1, 2, 3, \cdots, 2n \\ K_{ijl}^{vaa} & \text{for } p = 2n+1, \cdots, 4n \end{cases}$$

$$K_{pkl}^{ba} = \begin{cases} K_{ikl}^{wba} & \text{for } p = 1, 2, 3, \cdots, 2n \\ K_{ikl}^{wca} & \text{for } p = 2n+1, \cdots, 4n \end{cases}$$

Then, e_p is given as

$$e_p = \lambda^T (K_{pl}^{-a} g_l) - K_{ps}^{-a} K_{ijs}^{ab} a_i a_j = \lambda^T h_p - K_{ps}^{-a} K_{ijs}^{ab} a_i a_j$$

Substituting e_p in Eq. (7), we get the following equation:

$$\begin{aligned}K_{il} a_i - \lambda^T \bar{K}_{il}^g a_i + K_{pkl}^{ba} (\lambda^T h_p - K_{ps}^{-a} K_{ijs}^{ab} a_i a_j) a_k \\ + K_{ijkl}^{waaa} a_i a_j a_k = 0\end{aligned}$$

Rearranging the terms in the preceding equation, we get the final equation as

$$[K_{il} - \lambda^T (\bar{K}_{il}^g - K_{pil}^{ba} h_p)] a_i + (K_{ijkl}^{waaa} - K_{pkl}^{ba} K_{ps}^{-a} K_{ijs}^{ab}) a_i a_j a_k = 0$$

or

$$[K_{il} - \lambda^T K_{il}^g] a_i + K_{ijkl}^{\mathrm{NL}} a_i a_j a_k = 0$$

Acknowledgement

This work is done as a class project for the Structural Optimization course at Virginia Polytechnic Institute and State University. The authors wish to acknowledge the active support and advice by the instructor Zafer Gürdal.

References

[1] Dowell, E. H., "Nonlinear Oscillations of a Fluttering Plate," *AIAA Journal*, Vol. 4, No. 7, 1966, pp. 1267–1275.

[2] Dowell, E. H., "Nonlinear Oscillations of a Fluttering Plate II," *AIAA Journal*, Vol. 5, No. 10, 1967, pp. 1856–1862.

[3] Librescu, L., *Elastostatics and Kinetics of Anisotropic and Heterogenous Shell-type Structures*, Noordhoff International, Leyden, The Netherlands, 1975.

[4] Librescu, L., "Aeroelastic Stability of Orthotropic Heterogeneous Thin Panels in the Vicinity of the Flutter Critical Boundary, Part One: Simply Supported Panels," *Journal de Mécanique*, Vol. 4, No. 1, 1965, pp. 51–

76.
[5] Librescu, L., "Aeroelastic Stability of Orthotropic Heterogeneous Thin Panels in the Vicinity of the Flutter Critical Boundary, Part Two," *Journal de Mécanique*, Vol. 6, No. 1, 1967, pp. 133–152.
[6] Chatterjee, S. N., and Kulkarni, S. V., "Effects of Environment, Damping and Shear Deformations on Flutter of Laminated Composite Panels," *International Journal of Solids and Structures*, Vol. 15, No. 6, 1979, pp. 479–491.
[7] Oyibo, G. A., "Flutter of Orthotropic Panels in Supersonic Flow Using Affine Transformations," *AIAA Journal*, Vol. 21, No. 2, 1983, pp. 283–289.
[8] Birman, V., and Librescu, L., "Supersonic Flutter of Shear Deformable Laminated Composite Flat Panels," *Computers and Structures*, Vol. 139, No. 2, 1990, pp. 265–275.
[9] Dixon, I. R., and Mei, C., "Finite Element Analysis of Large-Amplitude Panel Flutter of Thin laminates," *AIAA Journal*, Vol. 31, No. 4, 1993, pp. 701–707.
[10] Marzocca, P., Lazzaro, R., and Librescu, L., "Flutter/Aeroelastic Response of Panels Via a Combined Galerkin-Volterra Approach," *45th AIAA/ASME/ASCE/AHS/ASC Structures, Structural Dynamics, and Materials Conference*, AIAA, Reston, VA, 2004, pp. 1–12.
[11] Lee, I., Lee, D. M., and Oh, I. K., "Supersonic Flutter Analysis of Stiffened Laminated Plates Subject to Thermal Load," *Journal of Sound and Vibration*, Vol. 224, No. 1, 1999, pp. 49–67.
[12] Liaw, D. G., "Supersonic Flutter of Laminated Thin Plates with Thermal Effects," *Journal of Aircraft*, Vol. 30, No. 1, 1993, pp. 105–111.
[13] Liaw, D. G., "Nonlinear Supersonic Flutter of Laminated Composite Plates Under Thermal Loads," *Computers and Structures*, Vol. 65, No. 5, 1997, pp. 733–740.
[14] Cheng, G., and Mei, C., "Finite Element Modal Formulation for Hypersonic Panel Flutter Analysis with Thermal Effects," *AIAA Journal*, Vol. 42, No. 4, 2004, pp. 687–695.
[15] Bolotin, V. V., *Nonconservative Problems of the Theory of Elasticity* , Macmillan, New York, 1963 (translated from Russian).
[16] Nagendra, S., Haftka, R. T., and Gürdal, Z., "Stacking Sequence Optimization of Simply Supported Laminates with Stability and Strain Constraints," *AIAA Journal*, Vol. 30, No. 11, 1992, pp. 2132–2137.
[17] Le Riche, R., and Haftka, R. T., "Optimization of Stacking Sequence Design for Buckling Load Maximization Using Genetic Algorithm," *AIAA Journal*, Vol. 31, No. 5, 1993, pp. 951–956.
[18] Kogiso, N., Watson, L. T., Gürdal, Z., and Haftka, R. T., "Genetic Algorithms with Local Improvement for Composite Laminate Design," *Structural Optimization*, Vol. 7, No. 4, 1994, pp. 207–218.
[19] Kogiso, N., Watson, L. T., Gürdal, Z., Haftka, R. T., and Nagendra, S., "Minimum Thickness Design of Composite Laminates Subject to Buckling and Strength Constraints by Genetic Algorithm," *35th AIAA/ASME/ASCE/AHS/ASC Structures, Structural Dynamics, and Materials Conference*, Vol. 14, AIAA, New York, 1994, pp. 2257–2275.
[20] McMahon, M. T., Watson, L. T., Soremekun, G., Gürdal, Z., and Haftka, R. T., "A Fortran 90 Genetic Algorithm Module for Composite Laminate Structure Design," *Engineering with Computers*, Vol. 14, No. 3, 1998, pp. 260–273.
[21] Soremekun, G., Gürdal, Z., Haftka, R. T., and Watson, L. T., "Composite Laminate Design Optimization by Genetic Algorithm with Generalized Elitist Selection," *Computers and Structures*, Vol. 79, No. 2, 2001, pp. 131–143.
[22] Venkataraman, S., and Haftka, R. T., "Structural Optimization Complexity: What Has Moore's Law Done For Us?," *Structural and Multidisciplinary Optimization*, Vol. 28, No. 6, 2004, pp. 375–387.
[23] Beiner, L., and Librescu, L., "Minimum-Weight Design of an Orthotropic Shear Panel with Fixed Flutter speed," *AIAA Journal*, Vol. 21, No. 7, 1983, pp. 1015–1016.
[24] Haftka, R. T., "Structural Optimization with Aeroelastic Constraints: A Survey of US Applications," *International Journal of Vehicle Design*, Vol. 7, Nos. 3–4, 1986, pp. 381–392.
[25] Librescu, L., Marzocca, P., and Silva, W. A., "Supersonic/Hypersonic Flutter and Postflutter of Geometrically Imperfect Circular Cylindrical Panels," *Journal of Spacecraft and Rockets*, Vol. 39, No. 5, 2002, pp. 802–812.
[26] Dowell, E. H., *Aeroelasticity of Plates and Shells*, Noordhoff International, Leyden, The Netherlands, 1975.
[27] Kuznetsov, Y. A., *Elements Of Applied Bifurcation Theory (Applied Mathematical Sciences)*, Springer, New York, 1998.
[28] Nayfeh, A. H., and Mook, D. T., *Nonlinear Oscillations*, Wiley, New York, and Institute of Electrical and Electronics Engineers, Los Alamitos, CA, 1995.
[29] Osyczka, A., *Evolutionary Algorithms for Single and Multicriteria Design Optimization*, Physica–Verlag, Heidelberg, Germany, 2002.
[30] Dowell, E. H., and Llgamov, M., *Studies in Non Linear Aeroelasticity*, Springer–Verlag, Berlin, 1988.

C. Pierre
Associate Editor